

## Treatment of Contaminated Water from Niger Delta Oil Fields with Carbonized Sisal Fibre Doped with Nanosilica from Ofada Rice Husk

Olayemi Abosede Odunlami<sup>1\*</sup>, Oluranti Agboola<sup>1</sup> Ebubechukwu Olive Odiakaose<sup>1</sup>,  
Oladipupo Oyindapo Olabode<sup>2</sup>, Oni Babalola<sup>1</sup>, Olubunmi Grace Abatan<sup>1</sup>,  
Isaac Owoicho<sup>1</sup>,

<sup>1</sup> Chemical Engineering Department, Covenant University, km 10 Idiroko Road, Ota, Ogun State, Nigeria

<sup>2</sup> Cummins West Africa Limited, Plot Y, Mobolaji Johnson Ave, Alausa, Lagos State, Nigeria

\* Corresponding author's email: olayemi.odunlami@covenantuniversity.edu.ng

### ABSTRACT

Oil spills contaminate water bodies and hence, cause the death of marine animals. The Niger Delta Oil contaminated water was treated by adsorption using sisal fibre activated carbon (SFAC) doped with silica nanoparticles (SNP) synthesized from Ofada rice husk which was carbonized at temperatures 400 °C and 650 °C. The SNP was synthesized at 600 °C (SNP-1) and 800 °C (SNP-2). The proportion in SFAC: SNP for both temperature values was 4.8:0.2 with a basis of 5 grams of the adsorbent. The samples were characterized by SEM, BET analysis, XRF and XRD. The adsorption equilibrium studies obeyed Langmuir adsorption isotherm; as the linear correlation value was close to unity, with a separation factor of 0.004. SNP-1 shows amorphous nature having Fe<sub>2</sub>O<sub>3</sub> and SNP-2 shows crystalline nature which consist of quartz. SNP-2 was used for the study due to its high surface area observed in the BET. High % removal efficiency of 99.84 was attained with silica nanoparticle (SNP-2) integrated in sisal fiber activated carbon (SFAC carbonized at 400 °C).

**Keywords:** adsorption; oil spills; sisal fibre; activated carbon; silica nanoparticle.

### INTRODUCTION

Oil spills had been a regular occurrence for about thirty years. It is one of the sources of pollution in water bodies. In addition, the levels of oil transport and weathering continues to rise due to such factors as salinity, temperature and tides [Doshi et al., 2018]. Statistics showed that the petroleum industry in Nigeria had raised its rate of oil spillage between 1976 and 2008 to around 80%. However, the growth of petroleum activities intensified oil spills and the consequent environmental degradation [Egwu, 2012]. The 2010 Deepwater Horizon oil spill brought approximately 4.9 million barrels of petroleum into the Gulf of Mexico. Various remedial techniques like chemical dispersing agents, mechanical booms and skimmers have been used to counter the risks of the leaked oil on the setting [Nyankson et al., 2015].

On exploration, transportation and processing of crude oil, the usage of its derivatives causes a risk of spillage with the potential of initiating significant environmental impact [Ewida, 2014]. Oil spills and chemical leaks occur regularly as oil production and marine traffic expand. Previous studies revealed that Europe suffered ten occurrences of petroleum spills in four decades, while in a decade, Nigeria witnessed 9,343 incidents [Kalejaiye, 2015]. This has made the nation one of the top five oil-damaged places in the world [Anejionu et al., 2015]. The pollution of water resulting from such incidents have resulted in significant environmental and ecological challenges and have been a threat to the climate, human health and national health [Liao and Wang, 2019].

The inefficient management of oil spills into seawater is an issue of considerable concern

worldwide. Increasing understanding of ecological and growing environmental policies worldwide has spurred great interest in developing cost-effective and reliable strategies for water-oil emulsions [Cambiella et al., 2006]. Contaminated water in the oil and gas industry consists of intricate organic pollutants such as radioactive substances, heavy metals and other heavy inorganic oils [Ghimire and Wang, 2018]. In addition, gasoline, diesel, and lubricating oils are products of petroleum refineries. These products are integral to a nation's economic development. However, the waste water from petroleum refinery contains many pollutants, such as heavy metals, volatile phenols, and polycyclic aromatic hydrocarbons [Abbas and Livingstone, 2018]. For example, among the natural compounds found in crude oil and petrol industries are petroleum hydrocarbons compounds which consists of benzene, toluene, ethylbenzene and xylene [Mohammadi et al., 2020]. These hydrocarbons are usually found in surface and underground water due to the activities in the industries, especially the procedure of handling of petrochemicals together with the reservoir leakage. As a result, these hydrocarbons are usually difficult to eliminate in the course of regular wastewater treatment processes [Pal et al., 2016; Wang et al., 2021].

Several mechanical, biological, and photochemical methods have been used to remedy this situation, Multiple methods, including a range of filters, reverse osmosis, gravity isolation, biological processes, chemical coagulation, ultra-filtration, electro flotation, and advanced oxidation process, are available to treat oil-contaminated water [Demirbas et al., 2017]. However, adsorption is the most frequently employed process among them [Burnstock, 2019]. Gupta and Tai (2016) found that in conjunction with being environmentally friendly, reusable, low density, and having excellent buoyancy properties, most sorbents are durable and chemically stable for handling spilt oil. For environmental applications, adsorption is an efficient technique, being considered one of the most suitable means for wastewater management. For environmental compatibility, green adsorbents are generated using agro-industrial waste as precursors. They are readily available, cost-effective, biodegradable, and non-toxic, making them suitable as sorbents in oil spill response [Wolok et al., 2020]. Such precursors

include sugarcane bagasse, palm kernel, rice straw, coconut shell, corncob, rice husk etc. However, a successful green adsorbent must have the required adsorption properties with the potential of regeneration [Rovani et al., 2018]. While the natural fibre in several industries generates more than 50% of the waste occupying extensive sites, the farm and biological waste fibre are still underutilized [Dungani et al., 2015]. It will be necessary for the industry to recycle these biomass and waste fibre such as rice husk, flax, sisal fibre, jute etc. into, new valuable products. They are activated carbon (AC) precursors and, because of their low cost (relative to commercial AC), accessibility and recyclability, are a great substitute [Cao et al., 2014]. The excellent adsorption efficiency of carbonized bio-materials is due to their large surface area and the high carbon content [Silvani et al., 2017].

Sisal Fibre, which is a precursor for producing AC, is extracted from the leaves of *Agave sisalana*. It is an essential source of fibres for composites due to its biodegradability, high tensile strength and versatility [Hajeeth et al., 2015]. Its wide application is due to easy cultivation. It is a high-cellulose fibre that contains both hemicellulose and lignin. Thus, it is highly likely to be used as a precursor for activated carbon [Nuriyah and Muafiqie 2017]. *Ofada* rice husk, on the other hand, is a by-product of the rice refining process (of Nigerian origin), which is the protective external shell of the rice grains. It is readily available, as it is produced in a yearly amount of about 120 million tons. They contain about 3% crude protein, 20% silica, 21% lignin, 21% hemicellulose, and 32% cellulose. They can be considered useful adsorbents due to their porous structure with plentiful floristic fibres, water insolubility and chemical properties [Jaman et al., 2009]. *Ofada* rice husk can be further processed into nano-silica for application in adsorption by several techniques such as the sol-gel method and the leaching and coprecipitation method.

Studies have shown that single adsorbents are not always sufficient alone in applications. Dawodu et al. (2020) used a feldspar-banana peel biochar composite as a low-cost, innovative adsorbent for removing crude oil from an aqueous medium. The prepared adsorbent brought forth a heterogeneous surface that exhibited improved hydrophobicity and

better adsorptive capacity for the adsorption of crude oil. An experiment was conducted by Malekmohammadi et al. (2016), who studied and compared silica, activated carbon, and zeolite adsorbents in the removal of ammonium, iron, COD, turbidity and phosphate pollutants. It also investigated the effect of discharge on the removal of contaminants. This experiment showed that silica has a high potential to extract adsorb iron and turbidity, reducing the concentrations to allowable levels. Silica also adsorbed ammonium, phosphorus, and COD, but not to an unacceptable level. Zeolite can adsorb ammonium and phosphate while reducing them to an allowable amount. However, its adsorptive capacity was relatively low when it acted on iron and COD. Activated carbon significantly reduced turbidity, COD, and other contaminants, not exceeding the maximum allowable drinking water amount.

It suggests that each adsorbent may eliminate a particular form of pollutant. It also depicts the probable lapses for each of the adsorbents while used separately, which now encourages the combination of the adsorbents for several applications. Thus, in this study, sisal fibre would be used as a precursor for making AC and is doped with synthesized silica nanoparticles from *Ofada* rice husk to treat the oil-contaminated water effectively. The leaching and co-precipitation method would be used to synthesize nano-silica, as *Ofada* rice husk is readily available for application. The efficiency of the application of adsorption in the treatment of contaminated water from the Niger Delta Oil fields would be studied using the sisal fibre-based AC alone and when doped with nano-silica synthesized from *Ofada* rice husk.

## MATERIALS AND METHODS

### Materials

The precursors used in preparing the adsorbents are sisal fibre and *Ofada* rice husk, both obtained in Ogun state, Nigeria. Phosphoric acid ( $H_3PO_4$ ) of 85% purity was used as an activating agent for preparing the Sisal Fibre Activated Carbon (SFAC). Distilled water was also utilized in washing the activated carbon until it was neutral. Sodium Hydroxide (NaOH) from Fischer, with 98.8 % purity and sulphuric acid ( $H_2SO_4$ ) from Sigma Aldrich, with 98 % purity were used in the synthesis of nano-silica from *Ofada* rice husk (RHA).

### Preparation of sisal fibre activated carbon (SFAC)

Sisal fibre was washed thoroughly with distilled water to remove impurities. The yarn was then dried in an oven at 120 °C to remove the water gained from washing. The washed fibre was cut to 2-3 cm in size and was wrapped tightly in aluminium foil to be heated at 250 °C in the oven until it was softer for grinding. The heated fibre was ground using a mortar and a pestle before carbonizing the two samples in a muffle furnace at 400 °C and 650 °C for 2 hours. Figure 1(a) shows a piece of carbonized fibre. The carbonized sisal fibre (SFC-1 and SFC-2) was activated chemically by impregnation with phosphoric acid (1 M  $H_3PO_4$ ) in a ratio of 3:1 (acid: precursor) for 24 hours. The produced activated carbon was then washed repeatedly with distilled water to remove the residual acid in the sample, as shown in Figure 1(b). This was done until there was an indication of a pH equal to 7. Then, the sample was dried in a hot air oven. The first activated carbon sample (SFAC-1) was prepared at

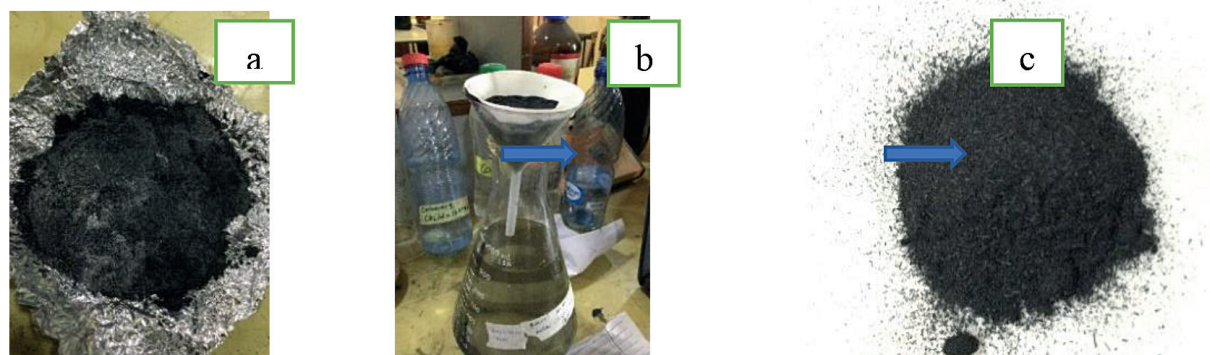


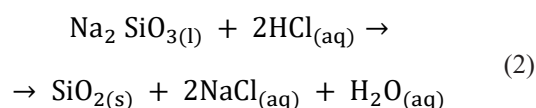
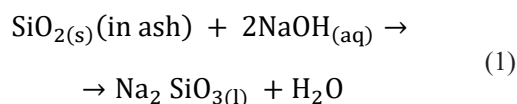
**Figure 1.** (a) Carbonized sisal fibre; (b) washing activating agent from carbon until neutral pH; and (c) activated carbon dried in the oven after washing out residual acid

400 °C while the second activated carbon (SFAC-2) was prepared at 600 °C. The sample of the prepared activated carbon is shown in Figure 1(c).

### Synthesis of silica nanoparticles (SNP)

The silica nanoparticles were prepared with the leaching and co-precipitation method [Jyoti et al., 2021]. The *Ofada* rice husk obtained from a rice mill was thoroughly washed to remove the contaminants present. It was then sun-dried for 12 hours before being thoroughly pulverized in a grinder and sieved to a size of 500 µm. The pulverized *Ofada* rice husk was divided into two samples; one was burnt at 600 °C for 4 hours and the other at 800 °C for 4 hours. The rice husk burnt at 600 °C is RHA-1, while the rice husk burnt at 800 °C is RHA-2. A pictorial representation of the burnt rice husk is shown in Figure 2(a). Burning the rice husk gave rise to the production of rice husk ash, RHA-1 and RHA-2. The sample was mixed with sodium hydroxide (1 M NaOH) and subjected to stirring at a constant speed at 80 °C for 2 hours, as shown in Figure 2(b). In the step mentioned above, the silica content in the rice husk ash was extracted with sodium hydroxide, yielding sodium silicate by filtration, as shown in Figure 2(c). Silica gel was obtained when the sodium silicate was further treated with sulfuric acid (1 M H<sub>2</sub>SO<sub>4</sub>) in Figure 2(d). This was carried

out by a dropwise addition of 1 M H<sub>2</sub>SO<sub>4</sub> to the sodium silicate with constant stirring at 50 °C. With the dropwise addition, the pH was monitored, and the formation of silica gel (see Figures 2 (e and f)) was observed at a pH of 8. The yield of silica gel was then dried for 2 hours at 200 °C in the oven to obtain silica nanoparticles. The silica obtained at 600 °C from RHA-1 is SNP-1, while the other obtained at 800 °C from RHA-2 is SNP-2. The silica nanoparticles are shown in Figure 2(g).



### Experimental batch study

A basis of 5 grams of adsorbent per 100 ml of wastewater was used for the sorption experiment. The adsorbent applied was SFAC doped with the two SNP in in the same proportions of 4.8:2 and only SFAC at 5:0. The wastewater was analyzed for the attainment of heavy metal concentrations. A hot plate magnetic stirrer was used for the adsorptive study with a contact time of 30, 60, 90

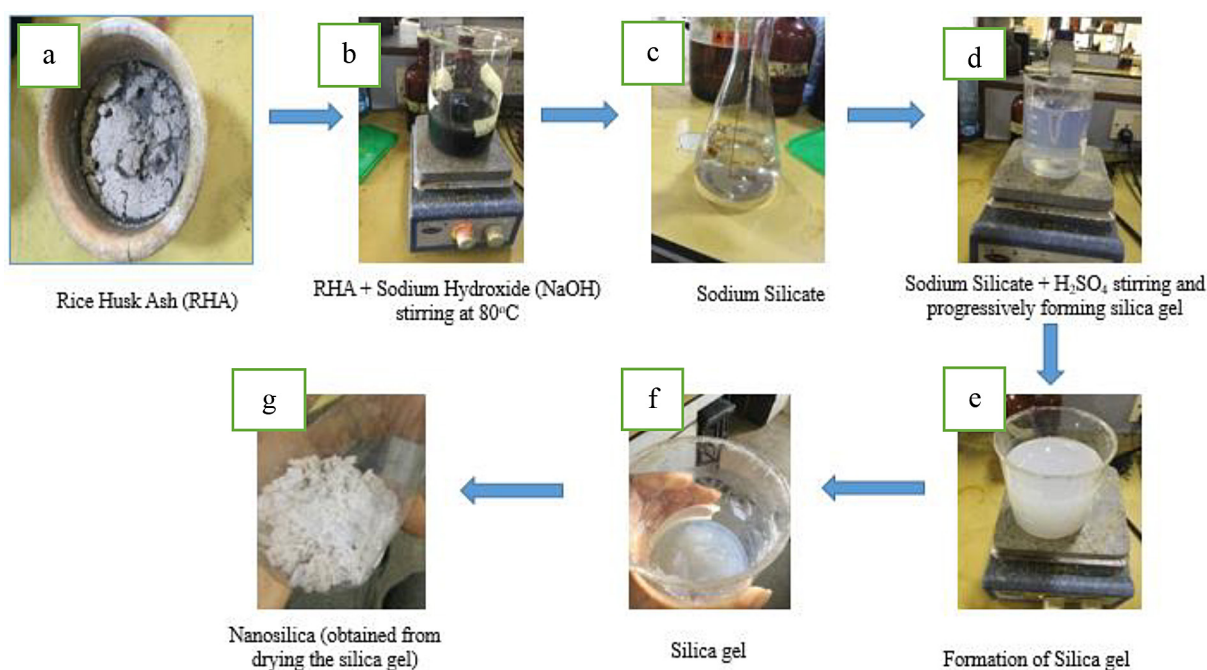


**Figure 2.** (a) Rice husk ash; (b) rice husk ash + NaOH stirring at 80 °C; (c) sodium silicate obtained as filtrate from the stirred mixture; (d) sodium silicate + H<sub>2</sub>SO<sub>4</sub> stirring and progressively forming silica gel; (e) formation of silica gel; (f) silica gel; and (g) nano-silica obtained by drying the silica gel in the oven

and 120 minutes for each run. The adsorption capacity was measured using the equation 3:

$$q_e = \frac{V * (C_o - C_e)}{M} \quad (3)$$

where:  $q_e$  is the adsorption capacity;  
 $V$  is the solution volume;  
 $M$  is the mass of adsorbent;  
 $C_o$  and  $C_e$  are the initial and equilibrium adsorbate concentrations, respectively.

### Adsorption isotherm

The Langmuir and Freundlich isotherms were applicable in investigating the behavior of the adsorption, as they provide some insight into the underlying adsorption mechanism and the affinity of the sorbent for the solute [Chowdhury et al., 2011]. The Langmuir and Freundlich isotherms are expressed in equations (4) and (5) respectively

$$\frac{C_e}{q_e} = \frac{1}{q_m K_L} + \frac{C_e}{q_m} \quad (4)$$

where:  $C_e$  is the equilibrium concentration of solute;  
 $q_e$  is the amount of solute adsorbed per unit weight of adsorbent;  
 $K_L$  is the adsorption capacity, or a monolayer capacity, and  $q_m$  is a constant.  
 The  $K_L$  can be used to calculate the separation factor,  $R_L$  which shows the extent to which the adsorption process is favorable

$$\text{Log } q_e = \text{Log } K_F + 1/n \text{ log } C_e \quad (5)$$

where:  $K_F$  and  $1/n$  are the constant characteristics of the system, the adsorption capacity and the adsorption intensity respectively.

The percentage removal efficiency (RE) was calculated using equation 6.

$$\%RE = \frac{C_i - C_f}{C_i} \times 100 \quad (6)$$

## RESULTS AND DISCUSSION

### BET surface area and yield

The BET surface area of the SFAC and SNP samples was calculated using a  $N_2$  adsorption-desorption isotherm at 77 K with a Micromeritics ASAP-2020 surface analyzer. Table 1 shows that a higher BET surface area was obtained when sisal fibre was carbonized at 650 °C as against 400 °C. This indicates a linear relationship between the BET surface area and the carbonization temperature. Dizbay-Onat et al. (2017) [29] also drew the same conclusions when the sisal waste activated carbon samples were prepared. The BET surface area increased from 1075.3  $m^2/g$  to 1245.3  $m^2/g$  with an increase in carbonization temperature from 550 °C to 650 °C. The total pore volume (in Table 4.1) has also depicted a linear relationship with the carbonization temperature of the SFAC samples. Burning the samples at higher temperatures will give room for the release of volatile matter, allowing the development of pores on the surface of the adsorbent.

According to Table 2 for the SNP samples, as the calcination temperature increased, total pore volume and BET surface area decreased. This clearly shows that increasing the calcination temperature reduced the pore volume, specific surface area, and porosity of the silica samples. However, from observation, increasing the calcination temperature increased the degree of crystallization of silica nanoparticles. The average pore diameter results have also shown that the mesoporous silica nanoparticles were synthesized from the Ofada rice husk. As a result of their high porosities, large surface areas, tunable pores and structural strength, mesopores are more efficient than macropores and micropores.

**Table 1.** BET surface area of the SFAC samples

Sample	BET surface area, $m^2/g$	Total pore volume, $cm^3/g$	Average pore diameter, nm
SFAC-1	980.260	0.5642	3.1672
SFAC-2	1230.250	0.6354	3.2454

**Table 2.** BET Surface Area for the Silica samples

Sample	BET surface area, $m^2/g$	Total pore volume, $cm^3/g$	Average pore diameter, nm
SNP-2	440.50	0.6044	3.2535
SNP-1	340.650	0.6020	3.1525

## X-ray fluorescence

The elemental analysis was accessed by X-ray fluorescence to determine the inorganic chemical composition of the samples, as shown in Tables 3 and 4. From these results, the silica content in the RHA samples and the purity of the silica samples were deduced. In Table 4.4, twelve compounds/elements were detected in the sample. RHA-1 and RHA-2 have shown the silica content up to 73.2% and 95.2%, respectively. This outcome can be attributed to the calcination temperature of the rice husk. Burning the rice husk at a higher temperature gave room for the loss of impurities in the sample, which maximized the silica content in the sample.

In the results from the XRF analysis, a higher percentage purity of silica was detected in SNP-1 (97.3%) compared to SNP-2 (94.5%). The XRD results for the silica samples have shown the crystalline phase (quartz) in SNP-1 and the presence of amorphous silica in SNP-2. From the experimental

**Table 3.** XRF for the rice husk ash samples, RHA-1 and RHA-2

Compounds (%)	RHA-1 (%)	RHA-2 (%)
SiO <sub>2</sub>	73.2	95.2
Al <sub>2</sub> O <sub>3</sub>	3.25	0.24
Fe <sub>2</sub> O <sub>3</sub>	1.75	0.12
MnO	0.67	0.05
CaO	4.35	0.80
P <sub>2</sub> O <sub>5</sub>	8.75	0.72
K <sub>2</sub> O	5.35	1.50
TiO <sub>2</sub>	0.25	0.01
MgO	0.3	0.45
Na <sub>2</sub> O	0.03	0.03
SO <sub>3</sub>	0.15	0.1
Others	<2.00	<0.8

**Table 4.** XRF for the silica samples, SNP-1 and SNP-2

Compounds/Elements	SNP-1 (%)	SNP-2 (%)
SiO <sub>2</sub>	97.3	94.5
Al <sub>2</sub> O <sub>3</sub>	0.5	0.24
Fe <sub>2</sub> O <sub>3</sub>	0.4	0.31
MnO	0.28	0.35
CaO	0.03	0.80
P <sub>2</sub> O <sub>5</sub>	0.2	0.72
K <sub>2</sub> O	0.4	0.95
TiO <sub>2</sub>	0.25	0.31
MgO	0.3	1.60
Na <sub>2</sub> O	0.34	0.22

procedure of synthesizing the silica nanoparticles, the rice husk ash (RHA-1 and RHA-2) from calcination was treated with sodium hydroxide to extract the silica in the form of sodium silicate. Therefore, the efficiency of this process is determined by the solubility of the silica in the alkaline medium. Amorphous silica is more soluble in alkaline media than crystalline silica, as its molecules are less tightly packed than the latter. This can also be subject to mass loss in the sample from burning at a higher temperature. On attaining the crystalline silica, stronger bonds are gained that aid the formation of coarse masses of silica and reduce its solubility in an alkaline medium.

## X-ray diffraction

The XRD patterns of the SNP-1 and SNP-2 are shown in Figure 3, which depicted the amorphous nature of SNP-1 having Fe<sub>2</sub>O<sub>3</sub> and the crystalline nature of SNP-2, mainly as quartz. The XRD patterns of SNP-1 show broad diffraction with a maximum intensity of around 22 °C, indicating the presence of amorphous silica in the sample. It further shows a characteristic broad band of ferrihydrate with d-value of 2.0 which is weak in Fe<sub>2</sub>O<sub>3</sub> with a predominate proportion of Fe. A slight peak was further developed in a budding with weak crystallization process. For SNP-2, the intense peaks of diffraction were shown with maximum intensity up to 5000, marking the prevalence of crystalline silica in the sample. This could be credited to calcining the Ofada rice husk at a higher temperature of 800 °C. However, with the crystalline phase, quartz in SNP-2, there is also an indication of magnesium oxide (MgO) at lower intensities. The prevalence of crystalline silica in the quartz form can also be accredited to the high surface area observed in BET (Table 2). Hence, only SNP-2 will be considered for further adsorption experiment because it is envisaged that there would be diffusion at the interface between the nanoparticle and the metal ions. SNP-2 depicted high surface area high average pore diameter.

## Scanning electron microscopy of SNP

The surface morphology and the porous structure of the synthesized silica nanoparticles are depicted in Figures 4a and 4b. Figure 4a represent 0.2 g silica nanoparticle (SNP-1) at 600 °C while Figure 4b shows 0.2 g silica nanoparticle (SNP-2) at 800 °C. The SEM images exhibited

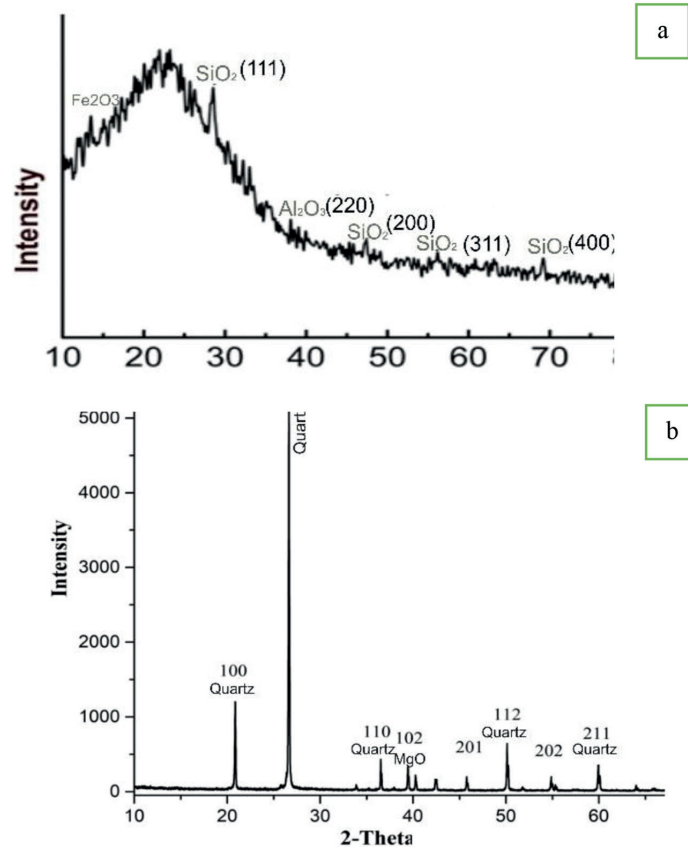


Figure 3. XRD Patterns for (a) SNP-1; and (b) SNP-2

different sizes of spherical particles with 0.2 g at 800 °C, showing smaller spherical particles. Both images displayed a favored size distribution and monodispersity, which contribute a crucial role in the formation of nanometer-scaled roughness [e] for the synthesis of silica nanoparticle from rice husk. The configuration of silica spheres forms several interspaces or cavities amid each sphere, which can roughen the surface of the rice husk in nanometer-scale [e]. In addition, SNP-1 shown in Figure 4a, the sphericity of the particles very

visible. For SNP-2, the accumulation of silica nanoparticles was established, thus developing larger coarse particles. This is attributed to calcining the Ofada rice husk at a higher temperature (800 °C over 600 °C) which aided the full development of the particles to coarse granular masses. This is confirmation of the XRD pattern observed in Figure 3b. Azmi et al. (2016) [30] confirmed this when they characterized silica derived from rice husk. Again, for this reason, only SNP-2 will be considered for further experiment.

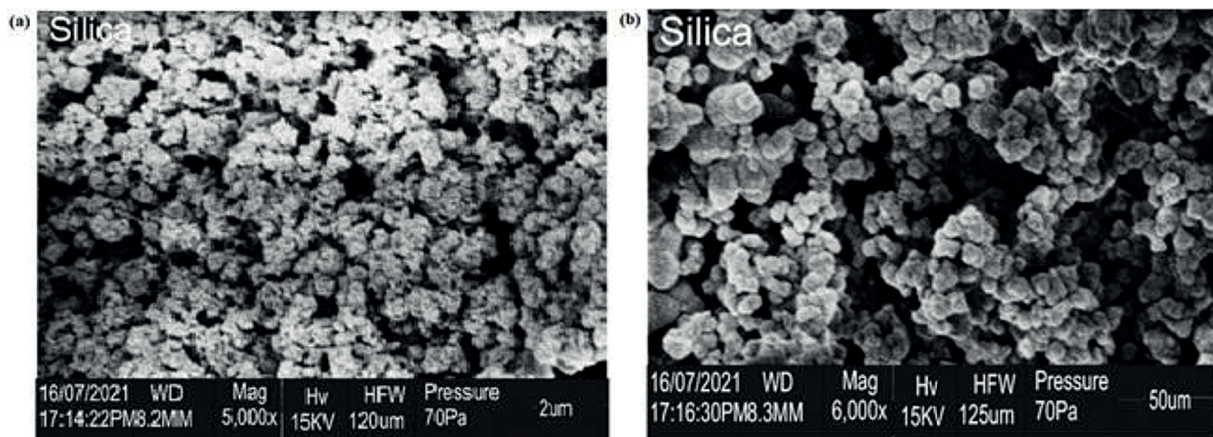


Figure 4. SEM micrograph of silica nanoparticle (a) SNP-1 and (b) SNP-2

### Scanning electron microscopy (SEM) of activated carbon composite

In the same vein, the surface morphology of sisal fiber activated carbon (SFAC) at different carbonization temperature and its composites with silica nanoparticle are depicted in Figures 4a, 4b, 4c, and 4d. All images in Figure 4 show a non-uniformity in the surface of the sample, with Figures 4a and 4b showing very little spherical particles. Some fibre-like strands are also observed in Figure 4a which was the sisal fiber carbonized at 400 °C, even whitish in color, indicating the ash content in the Figure. While the sisal fiber carbonized at 650 °C (Figure 4b) does not show a fiber-like strand nature; it shows more of ash content. The morphology in Figures 4c and 4d changed such that there was very little observable spherical particle in Figure 4c and no observable spherical particles in the samples in Figure 4d. With this, it is obvious there was an increase in surface area as a result of integrating silica

nanoparticle synthesized at higher temperature (800 °C) in the sisal fiber activated carbon. The increase in the surface area can be attributed to the to the high surface area observed in BET (Table 2), which will favour the adsorption process. Hence, for this study only the SNP-2 synthesized at higher temperature will be considered because it is expected that there would be diffusion at the interface amid the sisal fiber activated carbon (SFAC) with the integration of SNP-2 and the metal ion [Horsfall and Spiff, 2005].

### Effect of carbonization temperature on the SFAC/SFAC-SNP adsorbent for adsorption

The effect of carbonization temperature on the SFAC/SFAC-SNP adsorbent was studied using a basis of 5 grams of adsorbent for SFAC alone and 4.8 g:0.2 g of SFAC/SNP at different carbonization temperature (see Figure 6). It was observed from the results that the percentage removal efficiency of all the samples increase along with time. It was also observed

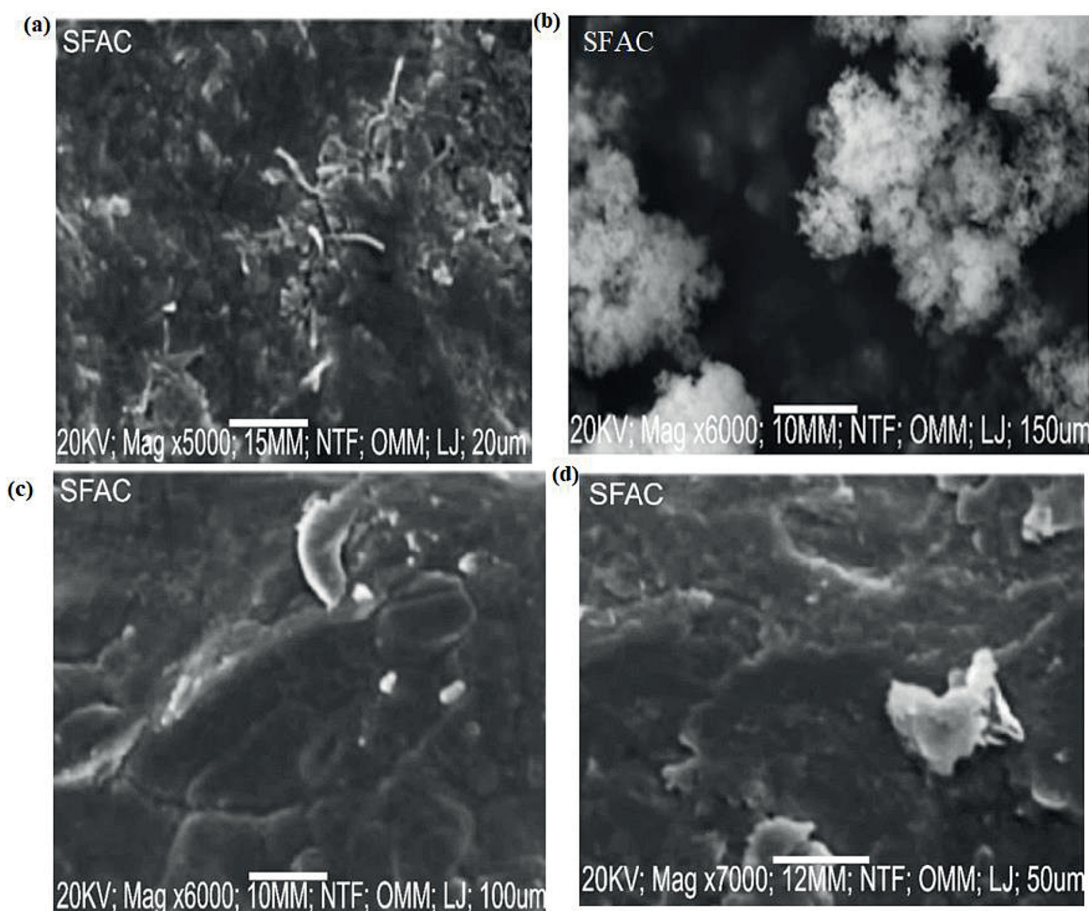


**Figure 5.** SEM micrograph of (a) sisal fiber activated carbon (SFAC; carbonized at 400 °C); (b) sisal fiber activated carbon (SFAC; carbonized at 650 °C); (c) SFAC carbonized at 650 °C-SNP-1; (d) SFAC carbonized at 400 °C -SNP-2

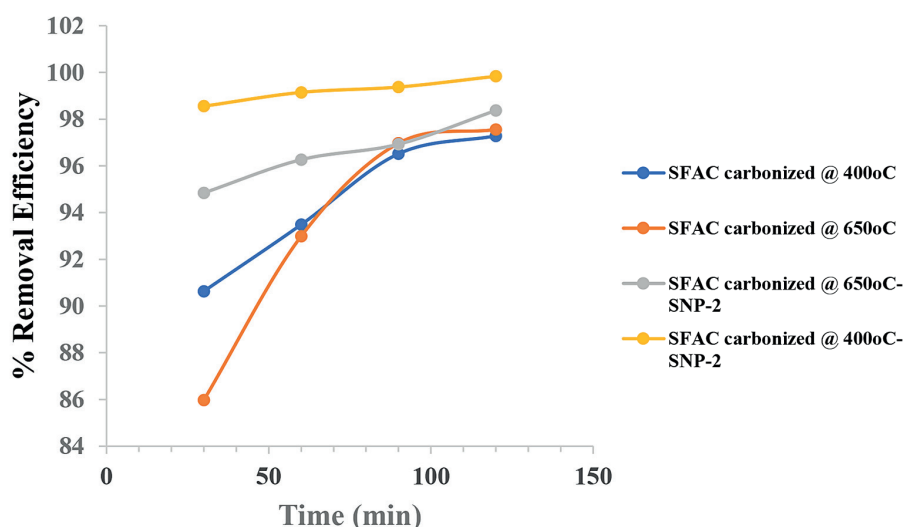


Figure 6. Removal Efficiency against time for SFAC/SFAC-SNP-2 adsorbent

that the silica nanoparticle (SNP-2) integrated in sisal fiber activated carbon (SFAC carbonized at 400 °C) gave the highest percentage removal efficiency at 120 min. This is attributed to the high surface area of the SNP-2 obtained from the BET analysis in Table 2. This result is in accordance with the theory of adsorption, which says that adsorption decreases with an upsurge in temperature and molecules initially adsorbed on a surface have the tendency to desorb from the surface at elevated temperatures [Zhang et al., 2012; Sanchez et al., 2021].

**Batch adsorption studies**

The concentration of observed in the wastewater when analyzed in shown in Table 5, while the final concentration is shown in Table 6. It was found the concentration of Cr decreases with increase in time of adsorption while the concentration of other metals found in the wastewater were completely removed. Hence, the adsorption study will only be based on chromium.

The adsorption process was studied with the Freundlich and Langmuir isotherms to check which data best fits. This inference was made from R<sup>2</sup> value from the graphs. For the Langmuir isotherm, a plot of C<sub>e</sub>/q<sub>e</sub> against C<sub>e</sub> to obtain a slope as 1/q<sub>m</sub> and an intercept of 1/q<sub>m</sub>K<sub>L</sub>. The Freundlich isotherm shows the plot of Log q<sub>e</sub> against Log C<sub>e</sub> to obtain a slope of 1/n and an intercept of Log K<sub>F</sub>. From Figure 7, the slope of the graph is 24.647 and q<sub>m</sub> was calculated as 0.0406. From the intercept, the Langmuir constant, K<sub>L</sub> was calculated as 101.6111. The separation factor R<sub>L</sub> was calculated to infer the affinity of the adsorbent for the adsorbate, which is 0.004. Because the R<sub>L</sub> value is less than one, it indicates that the adsorption of the metals unto the SFAC/SNP adsorbent is favorable. From Figure 8, the intercept of the graph, -1.2893, was used to obtain the value of K<sub>F</sub> as 0.0514, the value of n was also calculated from the slope of the graph as 6.274. Because the value of n is more significant than one, it demonstrates good adsorption

Table 5. Initial Concentration of metal ions in the wastewater

Metal ion	Cr	Pb	As	Mn	Cd	Ni
Concentrations (mg/L)	2.21	0.030	0.0001	0.022	0.002	0.01

Table 6. Removal concentration of metal ions in the wastewater at different time of adsorption process

Metal ion	Cr	Pb	As	Mn	Cd	Ni
Concentrations (mg/L)	30 min (0.034)	30 min (0)				
	60 min (0.034)	60 min (0)				
	90 min (0.007)	90 min (0)				
	120 min (0.002)	120 min (0)				

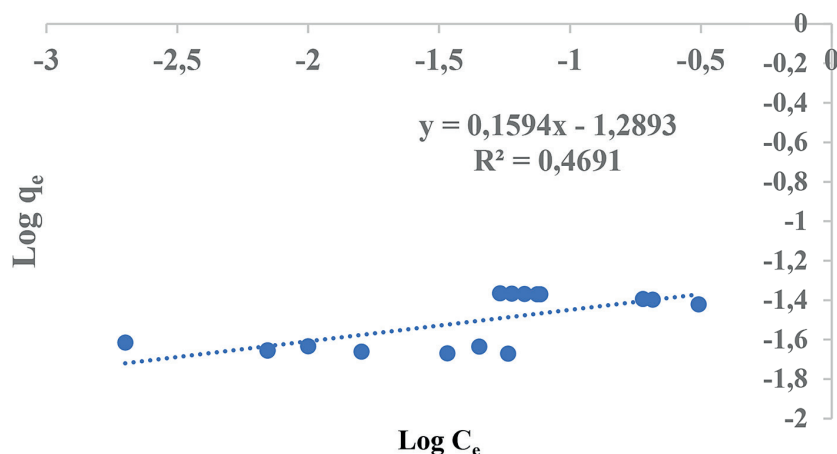


Figure 7. Freundlich Isotherm for Chromium metal

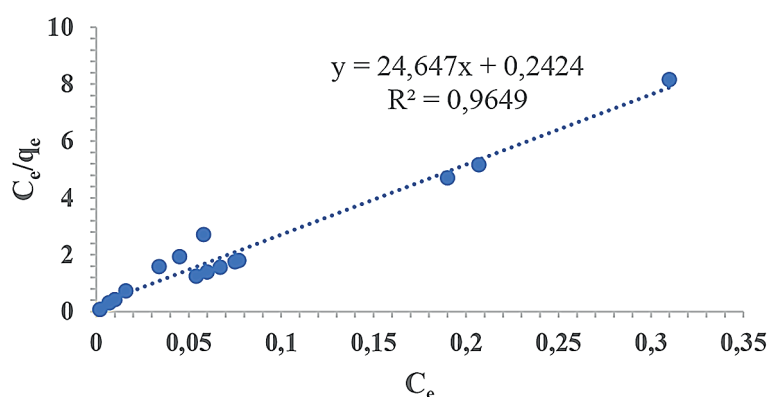


Figure 8. Langmuir Isotherm Model

through a physical process. This also indicates a weak adsorbate-adsorbent interaction, which may result from the distribution of surface sites on the adsorbent. The correlation coefficient ( $R^2$ ) values of Figure 8 have indicated- that the data best fits the Langmuir isotherm model, showing an  $R^2$  value of 0.9649 for the removal of hydrocarbon adsorption to the surface SFAC or SFAC/SNP.

## CONCLUSIONS

This study showed that the silica sample synthesized at a calcination temperature of 600 °C was amorphous while silica synthesized at a calcination temperature of 800 °C was crystalline. It was also observed that the amorphous silica synthesized at 600 °C has a lesser purity than the crystalline silica obtained at 800 °C, which was 94.5% and 97.3% respectively. Sisal Fibre Activated Carbon (SFAC) and SFAC-SNP-2 exhibited a high surface area, making it

a good adsorbent at carbonization temperature of 400 °C. The Sisal Fibre Activated Carbon doped with silica nanoparticles has been proven a suitable adsorbent for treating oil-contaminated water. The process was found more effective for the removal of chromium. In addition, other metals found in the wastewater were completely adsorbed. The adsorption process fits the Langmuir isotherm model, which shows that the adsorption is favorable, with a separation factor of 0.004. Thus, it has been recommended that silica nanoparticles be doped with sisal fibre activated carbon for the effective treatment of oil-contaminated water from Niger Delta Fields, as there was an observable decrease in pollutant concentration on the application of as little as 0.2 grams of silica nanoparticles.

## Acknowledgements

The authors acknowledge Covenant University for the financial support offered in the publication of this research.

## REFERENCES

- Doshi, B., Sillanpää, M. and Kalliola, S. 2018. A review of bio-based materials for oil spill treatment. *Water research*, 135, 262–277.
- Egwu, S.A. 2012. Oil Spill Control and Management. *Petroleum Technology Development Journal*, 2(1). [https://www.ptdjournal.com/?page\\_id=8](https://www.ptdjournal.com/?page_id=8)
- Nyankson, E., Rodene, D., Gupta, R.B. 2016. Advancements in crude oil spill remediation research after the Deepwater Horizon oil spill. *Water, Air, & Soil Pollution*, 227(1), 1–22.
- Ewida A.Y.I. 2014. Oil Spills: Impact on Water Quality and Microbial Community on the Nile River, Egypt. *The Handbook of Environmental Chemistry*, 3(4), 192–198. [https://doi.org/10.1007/698\\_2016\\_97](https://doi.org/10.1007/698_2016_97)
- Kalejaiye, K. 2015. Nigeria Records 9343 Oil Spill Incidents in 10 Years. *The Guardian*.
- Anejionu, O.C., Ahiamunnah, P.A.N., Nri-ezedi, C.J. 2015. Hydrocarbon pollution in the Niger Delta: Geographies of impacts and appraisal of lapses in extant legal framework. *Resources Policy*, 45, 65–77.
- Liao W., Wang Y.Z. 2019. Cellulose-Based Absorbents for Oil Contaminant Removal. *Cellulose-Based Superabsorbent Hydrogels*, 951–977. [https://doi.org/10.1007/978-3-319-77830-3\\_31](https://doi.org/10.1007/978-3-319-77830-3_31)
- Cambiella, A., Ortea, E., Rios, G., Benito, J.M., Pazos, C., Coca, J. 2006. Treatment of oil-in-water emulsions: Performance of a sawdust bed filter. *Journal of Hazardous Materials*, 131(1–3), 195–199.
- Ghimire, N., Wang, S. 2018. Biological treatment of petrochemical wastewater. In *Petroleum Chemicals-Recent Insight*, London, UK: IntechOpen, 55–74.
- Abbassi, B., Livingstone, T. 2018. A comparative review and multi-criteria analysis of petroleum refinery wastewater treatment technologies. *Environmental Research, Engineering and Management*, 74(4), 66–78.
- Mohammadi L., Rahdar A., Bazrafshan E., Dahmardeh H., Susan M., Hasan A.B., Kyzas G.Z., 2020. Petroleum hydrocarbon removal from wastewaters: A review. *Processes*, 8(4), 447.
- Pal, S., Banat, F., Almansoori, A., Abu Haija, M. 2016. Review of technologies for biotreatment of refinery wastewaters: progress, challenges and future opportunities. *Environmental Technology Reviews*, 5(1), 12–38.
- Wang, C., Chen, Z., Li, Y., Feng, K., Peng, Z., Zhu, Y., Yang, X. 2021. Refinery wastewater treatment via a multistage enhanced biochemical process. *Scientific Reports*, 11(1), 1–11.
- Demirbas, A., Bamuffeh, H.S., Edris, G., Alalayah, W.M. 2017. Treatment of contaminated wastewater. *Petroleum Science and Technology*, 35(9), 883–889.
- Gupta, S., Tai, N.H. 2016. Carbon materials as oil sorbents: a review on the synthesis and performance. *Journal of Materials Chemistry A*, 4(5), 1550–1565.
- Burnstock, A. 2019. Taking different forms: metal soaps in paintings, diagnosis of condition, and issues for treatment. In *Metal Soaps in Art*, Springer, Cham, 243–262.
- Wolok, E., Barafi, J., Joshi, N., Girimonte, R., Chakraborty, S. 2020. Study of bio-materials for removal of the oil spill. *Arabian Journal of Geosciences*, 13(23), 1–11.
- Rovani, S., Santos, J.J., Corio, P., Fungaro, D.A. 2018. Highly pure silica nanoparticles with high adsorption capacity obtained from sugarcane waste ash. *ACS omega*, 3(3), 2618–2627.
- Dungani R., Karina M.S., Sulaeman A., Hermawan D., Hadiyane A. 2015. Agricultural Waste Fibers Towards Sustainability and Advanced Utilization: A Review. *Asian Journal of Plant Sciences*, 15(1–2), 42–55. <https://doi.org/10.3923/ajps.2016.42.55>
- Cao, D., Shi, F., Koike, T., Lu, Z., Sun, J. 2014. Halophyte plant communities affecting enzyme activity and microbes in saline soils of the Yellow River Delta in China. *CLEAN–Soil, Air, Water*, 42(10), 1433–1440.
- Silvani, L., Vrchotova, B., Kastanek, P., Demnerova, K., Pettiti, I., Papini, M.P. 2017. Characterizing biochar as alternative sorbent for oil spill remediation. *Scientific Reports*, 7(1), 1–10.
- Hajeeth, T., Sudha, P.N., Vijayalakshmi, K. 2015. Removal of Cr (VI) from aqueous solution using graft copolymer of cellulose extracted from sisal fibre with acrylic acid monomer. *Cellul. Chem. Technol*, 49(9–10), 891–900.
- Nuriyah, S.R.A., Muafiqie, H. 2017. Analisis Pengaruh Produk Domestik Regional Bruto Dan Kemiskinan Terhadap Indeks Pembangunan Manusia Kabupaten Bojonegoro. *Journal of Public Power*, 1(2), 97–109.
- Jaman, H., Chakraborty, D., Saha, P. 2009. A study of the thermodynamics and kinetics of copper adsorption using chemically modified rice husk. *CLEAN–Soil, Air, Water*, 37(9), 704–711.
- Dawodu, F.A., Abonyi, C.J., Akpomie, K.G. 2021. Feldspar-banana peel composite adsorbent for efficient crude oil removal from solution. *Applied Water Science*, 11(1), 1–10.
- Malekmohammadi, S., Mirbagheri, A. and Ehteshami, M. 2016. Comparison of silica, activated carbon, and zeolite adsorbents in the removal of ammonium, iron, COD, turbidity and phosphate pollutants, and investigating the effect of discharge

- on the removal of pollutants. *International Journal of Humanities and Cultural Studies*.
27. Jyoti, A., Singh, R.K., Kumar, N., Aman, A.K., Kar, M. 2021. Synthesis and properties of amorphous nanosilica from rice husk and its composites. *Materials Science and Engineering: B*, 263, 114871.
  28. Chowdhury, S., Mishra, R., Saha, P., Kushwaha, P. 2011. Adsorption thermodynamics, kinetics and isosteric heat of adsorption of malachite green onto chemically modified rice husk. *Desalination*, 265(1–3), 159–168.
  29. Dizbay-Onat, M., Vaidya, U.K., Lungu, C.T. 2017. Preparation of industrial sisal fiber waste derived activated carbon by chemical activation and effects of carbonization parameters on surface characteristics. *Industrial crops and products*, 95, 583–590.
  30. Lin-Liu, Y.R., Chan, V.S., Chiu, S.C. 1996, February. Plasma rotation in the presence of radio frequency fields. In *AIP Conference Proceedings*. American Institute of Physics, 355(1), 247–250.
  31. Horsfall Jnr, M., Spiff, A.I. 2005. Effects of temperature on the sorption of Pb<sup>2+</sup> and Cd<sup>2+</sup> from aqueous solution by *Caladium bicolor* (Wild Cocoyam) biomass. *Electronic Journal of Biotechnology*, 8(2), 43–50.
  32. Zhang, M., Wang, S., Wang, C. and Li, J. 2012. A facile method to fabricate superhydrophobic cotton fabrics. *Applied Surface Science*, 261, 561–566.
  33. Sanchez, D.N., Knapp, C.W., Olalekan, R.M., Nanalok, N.H. 2021. Oil Spills in the Niger Delta Region, Nigeria: Environmental Fate of Toxic Volatile Organics.